Transp Porous Med
DOI 10.1007/s11242-014-0379-3

Joule–Thomson Effects on the Flow of Liquid Water

Philip H. Stauffer · K. C. Lewis · Joshua S. Stein · Bryan J. Travis · Peter Lichtner · George Zyvoloski

Received: 26 April 2014 / Accepted: 10 August 2014
© Springer Science+Business Media Dordrecht 2014

Abstract We present a revised form of the energy balance for the coupled thermodynamics of liquid water flowing in porous media and give examples of situations where a commonly used formulation based on transport of enthalpy leads to erroneous results. Assuming negligible contribution from kinetic energy as well as sources and sinks such as energy from radioactive decay, total energy conservation is reduced to a balance between changes in internal energy, enthalpy, conductive heat flux, and gravitational potential energy. The Joule–Thomson coefficient is defined as the change in temperature with respect to an increase in pressure at constant enthalpy. Because liquid water has a negative Joule–Thomson coefficient at low temperatures, at a constant gravitational potential water cools as it compresses and heats as it expands. If one ignores the gravitational energy, transport of enthalpy alone leads to water heating by 2°C per kilometer as it is brought up from depth. The corrected energy balance transports methalpy, which is enthalpy plus gravitational potential energy. Although the simpler form leads to small changes in the temperature profile for typical simulations, there are several instances where this effect may prove to be important. The most important impact of the erroneous form is probably in the field of geothermal energy production, where the creation of a few degrees of heat in a simulation could lead to miscalculation of power plant efficiencies.

Keywords Enthalpy · Methalpy · Gravitational energy · Energy balance · Mars

P. H. Stauffer and K.C. Lewis have contributed equally to this manuscript.

P. H. Stauffer · B. J. Travis · P. Lichtner · G. Zyvoloski
Los Alamos National Lab, Los Alamos, NM, USA

K. C. Lewis (✉)
Monmouth University, West Long Branch, NJ, USA
e-mail: klewis@monmouth.edu

J. S. Stein
Sandia National Laboratories, Albuquerque, NM, USA

Published online: 21 August 2014

1 Introduction

Advances in numerical modeling and computing speed over the past three decades have allowed the earth science community to explore many complex systems involving coupled heat and mass transfer in geologic systems. Examples include modeling of convection in oceanic crust [Fisher et al. (1990), Fisher and Hounslow (1990), Rees and Storesletten (1995)], groundwater flow near nuclear waste repositories (Pruess et al. 1990), geothermal energy [Hanano (1998), Weir (1994), Dempsey et al. (2012)], geyser behavior (Ingebritsen and Rojstaczer 1993), thermal development of oil fields, large scale lateral flow as found in both continental basins (Person et al. 1996) and submarine accretionary systems (Stauffer and Bekins 2001), planetary hydrologic studies [Travis et al. (2003), Travis et al. (2013), Palguta et al. (2010), Barnhart et al. (2010), Travis and Schubert (2005)], and geologic CO_2 storage (Deng et al. 2012).

The increased feasibility of coupled modeling and a wealth of applications have led to a proliferation of coupled heat and mass transfer codes formulated as finite difference or finite element/volume schemes. These codes generally account for the conservation of fluid energy in one of two ways. The first approach, which has been standard since the dawn of coupled heat and mass transfer modeling [Tsang (1999), Straus and Schubert (1977), Voss (1984)], avoids explicit use of internal energy or enthalpy in the energy balance equation by replacing these terms with approximate expressions involving the temperature.

The second approach is to write the energy balance in terms of fluid enthalpy and employs steam table data (Haar et al. 1984) to evaluate enthalpy as a function of both pressure and temperature [Lewis and Lowell (2009), Zyvoloski (2007), Travis et al. (1991), Hayba and Ingebritsen (1994)]. The enthalpy formulation more accurately captures the thermodynamic behavior of water. Moreover, enthalpy is often employed (together with fluid pressure) as a primary variable in two-phase problems involving pure water, because the temperature alone is insufficient to specify the amounts of steam and liquid water in thermodynamic equilibrium at a given pressure. However, the choice of pressure and enthalpy as primary variables may not extend easily to more general systems, for which it may be preferable to employ temperature, pressure, and volume saturation as primary. Either way, the inclusion of enthalpy in the energy balance is an improvement over using temperature alone. The enthalpy-based approach is especially valid in large scale models where large variation in the state variables leads to noticeable differences in fluid energy calculated by the enthalpy versus temperature-only approaches. While the enthalpy approach is completely valid for lateral flow systems, for vertical flow the method fails to account for changes in the gravitational potential energy of the water.

The issue concerning the effect of gravitational potential energy on fluid flow is not a new one, but it is severely underrepresented in the literature. One of the few discussions of which the authors are aware occurred when M.H. Dodson (1971) criticized D.R. Waldbaum (1971) inadvertant neglect of this term in the context of mantle convection. Recently, Manga and Kirchner (2004) noted the importance of including gravitational potential energy in their simulations of cold water springs.

In this paper, we review the appropriate form of the energy balance to use in conjunction with the fully coupled thermodynamics. Next, we present results obtained using gravitational corrected and uncorrected energy balances. Finally, we discuss broad implications of the fully coupled approach.

2 Theory

2.1 The Energy Equation for a Pure Fluid

The total energy balance for a volume of pure fluid in an Eulerian frame can be expressed as follows:

$$\frac{\partial}{\partial t}\int_V \left(\frac{1}{2}\rho v^2 + \rho g z + \rho u\right) dV = -\int_S \left(\frac{1}{2}\rho v^2 + \rho g z + \rho u\right) \mathbf{v}\cdot\hat{\mathbf{n}} dS - \int_S \mathbf{q}\cdot\hat{\mathbf{n}} dS - \int_S p\mathbf{v}\cdot\hat{\mathbf{n}} dS - \int_S (\underline{\underline{\tau}}\mathbf{v})\cdot\hat{\mathbf{n}} dS, \quad (1)$$

where ρ is the fluid density, $\mathbf{v}$ is the velocity, u is the specific internal energy, $\mathbf{q}$ is the conductive heat flux, p is the pressure, $\underline{\underline{\tau}}$ is the deviatoric stress tensor (i.e., the total stress tensor with the pressure subtracted from the diagonal), g is the gravitational acceleration, and the direction of increasing z coordinate is taken as positive upward. See Table 1 for a list

Table 1 Symbols employed, in order of their appearance in the text

Symbol	Meaning	Unit
t	Time	s
dV	Element of volume	m^3
ρ	Density	kg/m^3
v	Speed	m/s
$\mathbf{v}$	Velocity	m/s
g	Gravitational acceleration	m/s^2
z	Height	m
u	Specific internal energy	J/kg
dS	Element of surface area	m^2
$\hat{\mathbf{n}}$	Unit normal	none
$\mathbf{q}$	Heat flux	J/m^2s
p	Pressure	Pa
$\underline{\underline{\tau}}$	Deviatoric stress tensor	Pa
h	Specific enthalpy	J/kg
θ	Specific methalpy	J/kg
$\tilde{\lambda}$	Bulk thermal conductivity	W/m°C
T	Temperature	°C
ϕ	Porosity	none
k	Permeability	m^2
μ	Dynamic viscosity	Pa·s
μ_{JT}	Joule–Thomson coefficient	°C/Pa
α	Thermal expansivity	/°C
c_p	Specific heat (const. p)	J/kg°C
Φ	Defined as gz	m^2/s^2
s	Specific entropy	J/kg°C
d	Depth	km
D	Scale depth	km

of all the symbols employed in this paper together with their meanings and associated units. In words, Eq. (1) states that the rate of increase of the total energy (kinetic plus potential plus internal) of fluid in a volume V equals the rate at which the same quantity is added to the volume via convection, plus the rate at which heat is transferred to the volume via conduction, plus the rate at which volume work and viscous work are done on the fluid in V by the surrounding fluid. Even though in the Eulerian framework the volume considered remains stationary, the kinetic energy of the fluid within it may increase because the velocity of the fluid increases or because the density increases. Similarly, the potential energy will increase if the density of the fluid increases. Equation (1) can be shown to be equivalent to Eq. (11.1–7) from Bird et al. (1984) (see Appendix A for a derivation).

Eq. (1) can be written in terms of the quantity

$$\theta \equiv h + \frac{1}{2}v^2 + gz, \tag{2}$$

where h is the specific enthalpy. θ is referred to as the specific "methalpy" and, when multiplied by ρ, represents the enthalpy plus the kinetic and potential energies, all per unit volume. If we combine the term containing $p\mathbf{v}\cdot\mathbf{n}$ with the first term on the right hand side of (1) and use the fact that

$$u = h - \frac{p}{\rho}, \tag{3}$$

we obtain

$$\frac{\partial}{\partial t}\int_V (\rho\theta - p)\,\mathrm{d}V = -\int_S (\rho\theta)\,\mathbf{v}\cdot\hat{\mathbf{n}}\mathrm{d}S - \int_S \mathbf{q}\cdot\hat{\mathbf{n}}\mathrm{d}S - \int_S (\underline{\underline{\tau}}\mathbf{v})\cdot\hat{\mathbf{n}}\mathrm{d}S. \tag{4}$$

Using the divergence theorem to convert the surface integrals into volume integrals, the differential form of this equation is readily shown to be

$$\frac{\partial(\rho\theta - p)}{\partial t} + \nabla\cdot(\rho\mathbf{v}\theta) = -\nabla\cdot\mathbf{q} - \nabla\cdot\left[\underline{\underline{\tau}}\mathbf{v}\right]. \tag{5}$$

This equation represents energy balance in terms of methalpy. If the gravitational and kinetic energy terms are neglected, (5) becomes

$$\frac{\partial(\rho h - p)}{\partial t} + \nabla\cdot(\rho\mathbf{v}h) = -\nabla\cdot\mathbf{q} - \nabla\cdot\left[\underline{\underline{\tau}}\mathbf{v}\right]. \tag{6}$$

Although we have chosen to cast the energy balance in terms of enthalpy or methalpy, we emphasize two points. First, the use of these equations does not imply that enthalpy or methalpy need be chosen as primary variables. Second, we note that other approaches are possible. For example, by combining the energy equation with the Navier–Stokes equation, it is possible to cast the energy balance in terms of entropy (see Landau and Lifshitz (1987), pp. 193–194), which may carry an advantage in some situations [e.g., Kieffer and Delaney (1979) and Lu and Kieffer (2009)]; a correction for the gravitational potential energy could still be included.

In the Results section below, we will compare the accuracies of (5) and (6) in the context of flow in a porous medium, and relate our results to those of the classical Joule–Thomson experiment. Toward this end, in the next section, we derive the porous medium forms of these equations.

2.2 The Porous Flow Energy Equation

To derive the porous medium form of (5), we consider again Eq. (1), but now over a volume containing both fluid and solid phases. We assume that the solid phase is rigid, is not moving

as a whole, and is in thermodynamic equilibrium with the fluid. Furthermore, we neglect the work done by viscous forces internal to the fluid in comparison with other forms of work. Under these conditions, the energy balance may be written as

$$\frac{\partial}{\partial t}\int_{V_f}\left(\frac{1}{2}\rho_f v_f^2+\rho_f gz+\rho_f u_f\right)\mathrm{d}V_f+\frac{\partial}{\partial t}\int_{V_s}\rho_s u_s \mathrm{d}V_s$$
$$=-\int_{S_f}\left(\frac{1}{2}\rho v_f^2+\rho_f gz+\rho_f u_f\right)\mathbf{v}_f\cdot\hat{\mathbf{n}}dS_f-\int_S \mathbf{q}\cdot\hat{\mathbf{n}}\mathrm{d}S-\int_{S_f}p_f\mathbf{v}_f\cdot\hat{\mathbf{n}}\mathrm{d}S_f, \quad (7)$$

where the subscripts f and s refer to the fluid and solid phases. S_f refers to the part of the surface encompassing V that is in contact with fluid, while S refers to the whole surface enclosing the volume V. We assume that the heat flux is given by Fourier's law of heat conduction

$$\mathbf{q}=-\tilde{\lambda}\nabla T, \quad (8)$$

where T is the temperature, $\tilde{\lambda}$ is the bulk thermal conductivity of the solid plus fluid mixture, commonly given by (see Jorand et al. (2011) for other formulations)

$$\tilde{\lambda}=\phi\lambda_f+(1-\phi)\lambda_s, \quad (9)$$

and ϕ is the porosity, defined as

$$\phi=\frac{\mathrm{d}V_f}{\mathrm{d}V_f+\mathrm{d}V_s}=\frac{\mathrm{d}V_f}{\mathrm{d}V}. \quad (10)$$

Furthermore, we use (10) to re-write all of the integrals in (7) over the total volume and surface area as

$$\frac{\partial}{\partial t}\int_V\left(\frac{1}{2}\rho_f v_f^2+\rho_f gz+\rho_f u_f\right)\phi\mathrm{d}V+\frac{\partial}{\partial t}\int_V\rho_s u_s(1-\phi)\mathrm{d}V$$
$$=-\int_S\left(\frac{1}{2}\rho_f v_f^2+\rho_f gz+\rho_f u_f\right)\mathbf{v}_f\cdot\hat{\mathbf{n}}\phi\mathrm{d}S+\int_S\tilde{\lambda}\nabla T\cdot\hat{\mathbf{n}}\mathrm{d}S-\int_S p_f\mathbf{v}_f\cdot\hat{\mathbf{n}}\phi\mathrm{d}S, \quad (11)$$

where we have assumed that, just as $dV_f=\phi\mathrm{d}V$, we have $dS_f=\phi dS$. Because the solid phase is assumed to do no work, we may set u_s approximately equal to $c_{ps}T$, where c_{ps} is the specific heat at constant pressure of the solid phase. The quantity $\phi\mathbf{v}_f$ represents the volumetric flux of the fluid phase, which we will denote $\tilde{\mathbf{v}}_f$. Replacing $\phi\mathrm{v}_f$ with $\tilde{\mathbf{v}}_f$, u_s with $c_{ps}T$, and subjecting the terms in (11) to the the same steps that lead from (1) to (5) results in

$$\frac{\partial(\phi\rho_f\theta_f-\phi p_f)}{\partial t}+\frac{\partial[(1-\phi)\rho_s c_{ps}T]}{\partial t}+\nabla\cdot(\rho\tilde{\mathbf{v}}_f\theta_f)=\nabla\cdot(\tilde{\lambda}\nabla T). \quad (12)$$

Equation (5) takes this form for flow in a porous medium. The equation corresponding to (6) is thus

$$\frac{\partial(\phi\rho_f h_f-\phi p_f)}{\partial t}+\frac{\partial[(1-\phi)\rho_s c_{ps}T]}{\partial t}+\nabla\cdot(\rho\tilde{\mathbf{v}}_f h_f)=\nabla\cdot(\tilde{\lambda}\nabla T). \quad (13)$$

We will assume that the volumetric flux is governed by Darcy's law:

$$\tilde{\mathbf{v}}_f=-\frac{k_s}{\mu_f}\left(\nabla p+\mathbf{g}\cdot\nabla z\right), \quad (14)$$

where k_s is the permeability and μ_f is the dynamic viscosity. We note that the velocity in θ is still the fluid velocity, and not the volumetric flux $\tilde{\mathbf{v}}_f$, and also that our energy balances for the porous media case are less general than those derived above for a pure fluid. We have

made three primary assumptions. First, we have assumed that there are no heat sources such as radioactive substances or sources of electromagnetic radiation (when we used Fourier's law of conduction to replace **q**). Second, we have assumed a rigid solid matrix. Third, we have neglected viscous work in comparison with other forms of work done by the fluid.

2.3 The Joule–Thomson Coefficient

In the following sections, we will discuss simulation results in terms of the Joule–Thomson coefficient,

$$\mu_{\mathrm{JT}} \equiv \left(\frac{\mathrm{d}T}{\mathrm{d}p}\right)_h, \tag{15}$$

which can also be expressed as

$$\mu_{\mathrm{JT}} = (T\alpha - 1)\frac{1}{\rho c_p}. \tag{16}$$

Formula (16) follows from the derivation in Appendix B when g is set to zero. Here α is the thermal expansivity at constant pressure and c_p is the specific heat at constant pressure (Pippard 1957). For water, μ_{JT} is negative at temperatures below approximately 250°C, which implies an increase in temperature of approximately 2.2 °C per 10 MPa drop in pressure at 20 °C for a constant enthalpy process. Wood and Spera (1984) highlight the importance of the same effect in connection with adiabatic decompression of certain geologic aqueous fluids. For example, they show that for salt water the increase in temperature with decreasing pressure can be even more pronounced. Figure 1 shows the magnitude of the Joule–Thomson coefficient as a function of temperature at four different pressures, generated from the NIST/ASME Steam properties database version 2.2 (2002). We note also that for the non-ideal gases hydrogen and helium (where α does not equal 1/T), μ_{JT} is negative at room temperature, causing decompressing hydrogen to heat (Kestin 1979).

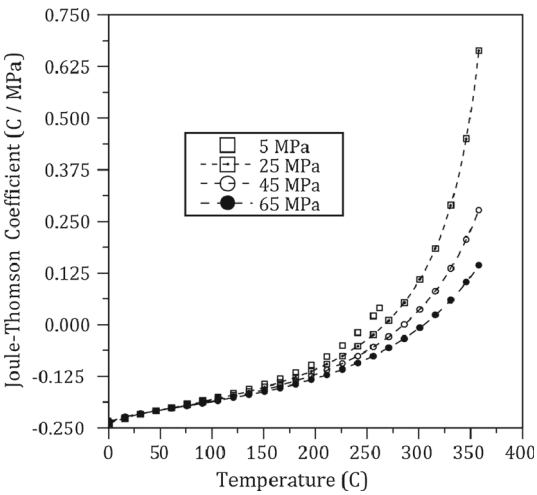

Fig. 1 Increase in the Joule–Thomson coefficient as a function of temperature and pressure

3 Examples and Discussion

The need to include gravitational potential energy in certain fluid flow calculations was exemplified by an error in the authors' own code. Oceanic bottom water is quite near the freezing point, so that neglecting the potential energy and thus miscalculating the pressure/temperature relationship of sinking fluid can lead to water spuriously freezing as it flows into the crust from the seafloor. Fluid freezing caused the finite-element code FEHMN (Zyvoloski 2007) to crash as the temperature went beyond the expected limits of the fluid property lookup tables.

In this section, we present simple simulations that clearly show the differences in solution behavior when the corrected (12) versus the uncorrected (13) energy balances are employed. Simulations are run using FEHMN and the integrated finite-difference code MAGHNUM [Travis et al. (1991), Travis et al. (2003), Travis et al. (2012)] with modifications to explore the effects of using different formulations of the energy balance. The unmodified codes use the enthalpy formulation (13); to incorporate (12), we add the gz term in the appropriate subroutine. In both cases, the enthalpy is calculated using a lookup table in which fluid enthalpy is given as a function of temperature and pressure.

The first important case involves the rapid removal of water from depth in geothermal energy production simulations. Simulations employing only the enthalpy formulation of the energy balance (13) could add more than 2°C per kilometer in the extracted water relative to simulations using the methalpy formulation, leading to overestimates of energy efficiencies for a geothermal power plant. Such overestimation could have potentially devastating consequences for the economic feasibility of such installations.

We model upward flow driven by a fixed pressure gradient. The domain is a two-dimensional box, 1,000 m on each side, composed of a homogeneous porous medium. The computational grid consists of 2500 nodes with a spacing of approximately 4 m in both the horizontal and vertical directions. The bottom of the domain ($z = 0$) is fixed at 11.5 MPa and 2 0°C, while the top of the domain ($z = 1{,}000$ m) is fixed at 1.0 MPa and 20 °C. The sides of the system are subject to zero heat and zero mass flux boundary conditions. Permeability is set to 10^{-10} m^2, porosity is set to 0.2, and thermal conductivity is set to 0.1 W/(m K) to limit thermal conduction effects. Via Darcy's law these parameters generate a one-dimensional upward volume flux of $q = 6.3 \times 10^{-5}$ m/s. With this reference setup, we run simulations with FEHM using the enthalpy formulation (13) and again using the methalpy formulation (12). For an inter-code comparison, the simulations are repeated using MAGHNUM. In these simulations, we neglect the kinetic energy part of θ. This is justified because the relevant velocities are small, and thus the velocity squared is of second order smallness. On the other hand, the potential energy term remains non-negligible. The results of these simulations are shown in Fig. 2.

To understand these results, we note that (13) takes the approximate form

$$\frac{\partial(\rho v h)}{\partial z} \approx 0, \tag{17}$$

because the initial temperature and pressure profiles are already steady state solutions of the mass and energy balance equations. Equation (17) implies that the enthalpy is approximately constant throughout the column, as the volumetric flux is constant and the liquid density is approximately constant. The constancy of the enthalpy implies that the Joule–Thomson coefficient can be used to calculate the temperature difference between the bottom and top of the system. An average value of μ_{JT} for this system is about -0.22 °C/MPa, which combined with a decrease in pressure of about 10 MPa should result in a temperature increase of about 2.2 °C. This increase is evident in Fig. 2 for the simulations using the enthalpy-based energy

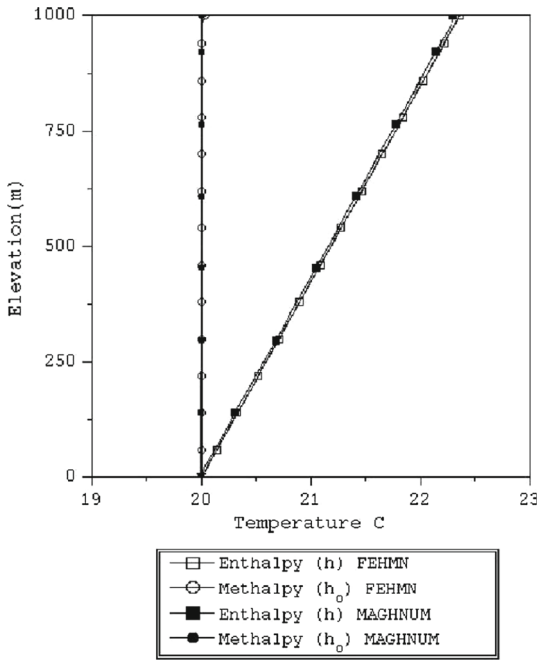

Fig. 2 Temperatures with elevation in simulations of upflow in a 1 km stack of porous material

balance. In contrast, Eq. (12) takes the approximate form

$$\frac{\partial(\rho v\theta)}{\partial z} \approx 0, \tag{18}$$

and a similar argument to that above shows that θ is approximately constant throughout the column. Therefore, in this case, the relevant quantity for calculating the increase in temperature from the bottom to the top is

$$\left(\frac{\partial T}{\partial p}\right)_\theta = \mu_{JT} - \frac{g}{c_p}\left(\frac{\mathrm{d}p}{\mathrm{d}z}\right)^{-1}. \tag{19}$$

We prove this relation in Appendix B, and for brevity refer in general to those parts of fluid temperature changes represented by (16) or (19) as "Joule–Thomson effects." For the parameters in our simulations, the term in (19) involving gravity almost exactly cancels μ_{JT}, explaining why the temperature is constant in the column when the methalpy formulation is employed. Finally, because both of the above simulations are focused on the steady state, we note that the results are not sensitive to different permeabilities or pressure gradients (as long as the pressure does not vary over such a large range that the density is no longer approximately constant in the column).

For the second case, we made a comparison between the enthalpy versus methalpy formulations for a thermal convection simulation. This particular simulation is from a study of a hypothetical aquifer on Mars (Travis et al. 2003). Apart from reduced gravity, similar conditions could be found on Earth (for much shallower systems). The Martian aquifer simulation is ideal for testing differences between the two formulations because of the low temperature gradient that exists over a large vertical distance. A 2-D geometry, 10 km wide and 10 km deep, with depth-dependent permeability and porosity is subjected to a constant bottom heat flux of 30 mW/m^2, while the surface temperature is maintained at 10 °C.

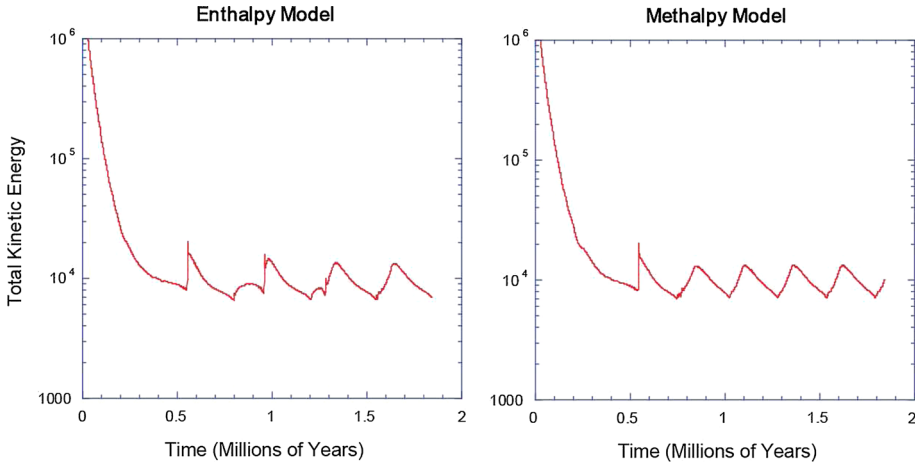

Fig. 3 Comparision of kinetic energy versus time in a 10 km × 10 km convection cell, enthalpy versus methalpy formulations

The porosity and permeability in the Martian subsurface are assumed to decrease exponentially with depth, as is observed in Earth systems, dropping from that of loose soil at the surface to that of unfractured igneous and metamorphic rock at 10 km depth. Following a model widely used in the planetary science community, the permeability is taken to vary according to

$$k = k_0 e^{-3d/D}, \tag{20}$$

where D is a scale depth of 2.8 km, d is depth in km, and the naught subscript refers to the surface value; similarly, porosity varies as

$$\phi = \phi_0 e^{-d/D}. \tag{21}$$

Travis et al. (2003) perform a parameter study in which permeability and porosity are varied along with other variables. For the following example, we use a surface permeability of 10^{-10} m^2 (corresponding to sand/sandy gravel) and a surface porosity of 35 %. The permeability decreases to about 2×10^{-15} m^2 and the porosity to slightly less than 1 % by 10 km depth. The average permeability over the total depth is about 2.4×10^{-14} m^2, while the average porosity is about 5 %.

The simulations based on the enthalpy and methalpy formulations differ in noticeable ways. Figure 3 shows the total system kinetic energy versus time. After an initial strong overturn, both formulations exhibit oscillations. For the methalpy formulation, the oscillations follow a regular period, while for the enthalpy formulation, the oscillations are not characteristic of a single frequency. The average magnitude is about the same in both formulations; however, the two formulations are out of phase by the end of the simulation time (1.89 Ma). Figure 4 shows the horizontally averaged temperature versus depth after 1.89 Ma of simulation time for the two formulations with significant differences apparent. The methalpy case is generally warmer, with a higher average basement temperature. The enthalpy formulation curve is 3–4 °C cooler throughout the interior region. Figure 5 shows color-coded plots of the temperature distribution after 2 Ma of simulation time for the two cases, with the color range representing 8°C (violet) to 60 °C (red). The patterns are not identical, and these plots corroborate the information in the kinetic energy plots that show the two cases are not in

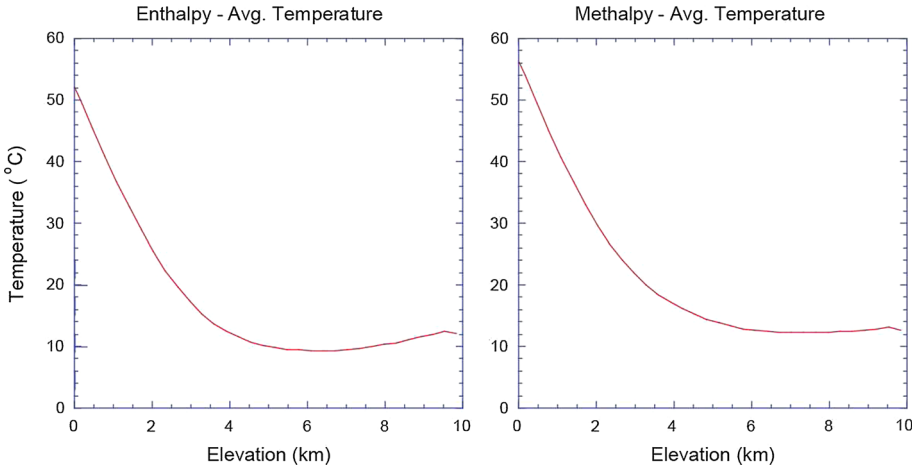

Fig. 4 Comparison of the horizontally averaged temperature in 10 km × 10 km convection cell at 1.89 Ma, enthalpy versus methalpy

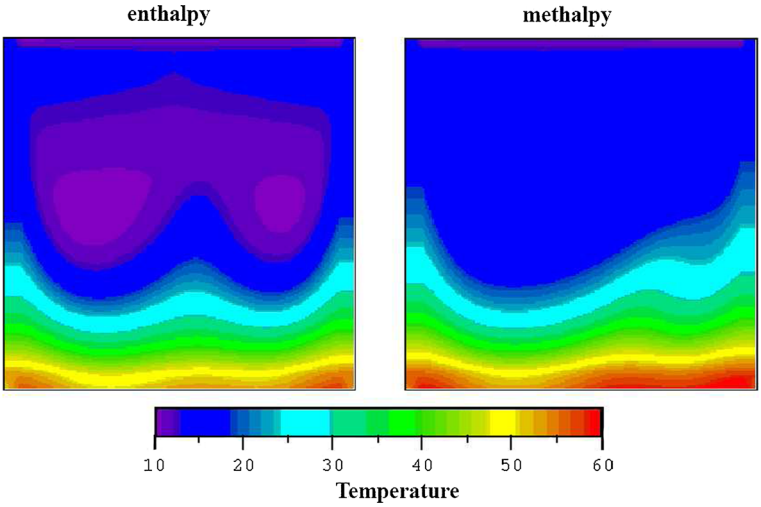

Fig. 5 Temperature contours in a 10 km × 10 km convection cell at 1.89 Ma, enthalpy versus methalpy formulations

the same phase after 1.89 Ma of simulation time. The warmer interior and basement for the methalpy formulation are again evident.

We now derive a criterion that is sufficient to determine when the gravitational energy can be neglected in the energy balance. Subtracting the left hand side of (6) from that of (5) gives the remainder

$$\frac{\partial(\rho g z)}{\partial t} + \nabla \cdot (\rho g z \mathbf{v}), \tag{22}$$

and gravitational energy can be neglected if these terms are small compared to the corresponding terms

$$\frac{\partial}{\partial t}\left(\rho h + \frac{1}{2}\rho v^2\right) + \nabla \cdot \left[\left(\rho h + \frac{1}{2}\rho v^2\right)\mathbf{v}\right]. \tag{23}$$

Let $\Delta\rho$, $\Delta(\rho h)$, and $\Delta(\rho v^2)$ be the largest changes in these quantities over either the characteristic temporal or spatial scales involved in a problem. Then the gravitational potential energy can be neglected if

$$\frac{gz\Delta\rho}{\Delta(\rho h) + \frac{1}{2}\Delta(\rho v^2)} = \frac{gz}{\frac{\Delta(\rho h)}{\Delta\rho} + \frac{1}{2}\frac{\Delta(\rho v^2)}{\Delta\rho}} \ll 1. \tag{24}$$

As expected, this relation will not hold if z or the gravitational acceleration is too large, though the domain over which z may vary is increased if either of the fractional terms in the denominator is large.

In addition to the cases presented above, the following examples highlight areas that may be of further interest:

- Lateral flow driven by large horizontal pressure gradients arising from plate tectonics could lead to water heating as it flows from high to low pressure regions. This process may help to explain high temperatures found in fluids in the toe regions of accretionary prisms (Fisher and Hounslow 1990).
- Flow in overpressured hydrocarbon traps.
- Flows impacting the stability of seafloor methane hydrates.
- Geologic CO_2 sequestration (Pruess 2008), especially industrial-scale CO_2 storage (Deng et al. 2012).
- Flows that occur near a phase transition.
- Flows that include chemical and biological reactions (biogeochemical reactions are generally very sensitive to temperature).

We have shown that there are important situations where geoscientists must be aware of Joule–Thomson effects and be able to knowledgeably model conservation of energy. Because of the non-linear relationship between pressure, temperature, and the Joule–Thomson coefficient combined with competing effects of thermal conductivity and flow rate, we suggest that simulations performed with an incorrect energy balance should be examined on a case-by-case basis to determine the significance of the correction.

As shown in the examples, the addition of a gravity term to the conservation of energy equation can produce significantly different results when, during a simulation, fluid travels large distances vertically. The term is easy to add to an existing simulator by including the gravity $\times$ height term immediately after the enthalpy of any fluid is calculated. The same term must also be added to any energy boundary conditions, but only for conditions that produce inflow. Because the added term is constant in time and never depends on any independent variable, performance of any iterative solution method (e.g., Newton–Raphson) is unaffected. Similarly, extension of our approach to 3D should pose no new problems; investigations of 3D effects due to inclusion of the gravitational potential in the energy balance may be worthy of future study.

4 Conclusions

We have presented the correct form of the energy balance to use when modeling the fully coupled thermodynamics of liquid water, and shown that this formulation involves methalpy in place of enthalpy, the methalpy including a term for gravitational potential energy. Furthermore, we have shown that there are important situations where geoscientists must be aware

of Joule–Thomson effects and be able to correctly model conservation of energy. Without the correction for gravitational potential energy, models can exhibit strange behavior due to spurious Joule–Thomson effects. Oceanic bottom water being drawn down into a fractured system will cool by approximately 2 °C per kilometer and simulations of focused convection into the seafloor may lead to freezing, a result that is not physically realistic. More importantly, miscalculation of withdraw temperatures for geothermal power plants using an incorrect form of the energy balance may impact calculated operating efficiencies. Additionally, Martian groundwater convection simulations were used to compare enthalpy- and methalpy-based energy balances in an environment that helps to accentuate the differences between the two formulations. The comparison shows that the methalpy formulation can lead to noticeably different results, including the temperature distribution within the domain and the character of long-term oscillations in the total kinetic energy of the system.

The corrected energy balance does exhibit Joule–Thomson effects in both vertical and horizontal fluid flow. These effects may be important for understanding heat flow in accretionary prisms or continental collision zones. Simulations of fluid flow and chemical transport near overpressured oil reservoirs may also be affected by Joule–Thomson effects.

Finally, the non-linear relationship between pressure, temperature, and the Joule–Thomson coefficient combined with competing effects of thermal conductivity and flow rate lead us to suggest that simulations performed with an incorrect energy balance should be examined on a case-by-case basis to determine the significance of the correction.

Acknowledgments We thank Quentin Williams and Satish Karra for their input to the theoretical discussions of this problem. We also thank Nina Rosenberg and Andy Fisher for their help in identifying this phenomenon during a modeling study of seafloor convection. Finally, we acknowledge funding from the US-China Advanced Coal Technology Consortium (under the management of West Virginia University).

Appendix A

Equation (11.1-7) from Bird et al. (1984) is, in our notation,

$$\frac{\partial}{\partial t}\left[\rho\left(u+\frac{1}{2}v^2\right)\right] = -\nabla\cdot\left[\rho\mathbf{v}\left(u+\frac{1}{2}v^2\right)\right] - \nabla\cdot\mathbf{q} - \nabla\cdot(p\mathbf{v}) - \nabla\cdot(\underline{\underline{\tau}}\mathbf{v}) + \rho(\mathbf{v}\cdot\mathbf{g}). \quad (25)$$

If we define

$$\Phi \equiv gz \quad (26)$$

then the term $\rho(\mathbf{v}\cdot\mathbf{g})$ can be written as

$$\rho(\mathbf{v}\cdot\mathbf{g}) = -\rho\mathbf{v}\cdot\nabla\Phi = -\nabla\cdot(\rho\mathbf{v}\Phi) + \Phi\nabla\cdot(\rho\mathbf{v}). \quad (27)$$

On the other hand, the mass balance equation for the fluid is

$$\frac{\partial\rho}{\partial t} + \nabla\cdot(\rho\mathbf{v}) = 0. \quad (28)$$

Solving (28) for $\nabla\cdot(\rho\mathbf{v})$ and substituting the result into the rightmost term in (27) yields

$$\rho(\mathbf{v}\cdot\mathbf{g}) = -\nabla\cdot(\rho\mathbf{v}\Phi) - \Phi\frac{\partial\rho}{\partial t} = -\nabla\cdot(\rho\mathbf{v}\Phi) - \frac{\partial(\Phi\rho)}{\partial t}. \quad (29)$$

Substituting (29) into (25) and rearranging yields

$$\frac{\partial}{\partial t}\left[\rho\left(u+\frac{1}{2}v^2+\Phi\right)\right] = -\nabla\cdot\left[\rho\mathbf{v}\left(u+\frac{1}{2}v^2+\Phi\right)\right] - \nabla\cdot\mathbf{q} - \nabla\cdot(p\mathbf{v}) - \nabla\cdot(\underline{\underline{\tau}}\mathbf{v}). \quad (30)$$

Integrating this equation over a volume V and using the divergence theorem on all terms involving ∇ results in (1).

Appendix B

From Eq. (2), and neglecting the kinetic energy term, the differential of θ is

$$\mathrm{d}\theta = \mathrm{d}h + g dz. \tag{31}$$

Using the definition $h \equiv u + p/\rho$, it is easy to show that

$$\mathrm{d}h = T\mathrm{d}s + \frac{1}{\rho}\mathrm{d}p, \tag{32}$$

where s is the specific entropy. Moreover, considering s as a function of temperature and pressure leads to

$$\mathrm{d}s = \left(\frac{\partial s}{\partial T}\right)_p \mathrm{d}T + \left(\frac{\partial s}{\partial p}\right)_T \mathrm{d}p \tag{33}$$

Combining (31), (32), and (33) results in

$$\mathrm{d}\theta = T\left(\frac{\partial s}{\partial T}\right)_p \mathrm{d}T + \left[T\left(\frac{\partial s}{\partial p}\right)_T + \frac{1}{\rho}\right]\mathrm{d}p + g dz. \tag{34}$$

Using the identity

$$T\left(\frac{\partial s}{\partial T}\right)_p = \left(\frac{đQ}{\mathrm{d}T}\right)_p \equiv c_p, \tag{35}$$

and the Maxwell relation

$$\alpha\rho \equiv \left(\frac{\partial \rho}{\partial T}\right)_p = -\left(\frac{\partial s}{\partial p}\right)_T, \tag{36}$$

equation (34) becomes

$$\mathrm{d}\theta = c_p \mathrm{d}T + (1 - \alpha T)\frac{\mathrm{d}p}{\rho} + g\mathrm{d}z. \tag{37}$$

Hence, for a constant methalpy process we have

$$\left(\frac{\partial T}{\partial p}\right)_\theta = (T\alpha - 1)\frac{1}{\rho c_p} - \left(\frac{g}{c_p}\frac{\mathrm{d}p}{\mathrm{d}z}\right)^{-1} \equiv \mu_{JT} - \frac{g}{c_p}\left(\frac{\mathrm{dp}}{\mathrm{d}z}\right)^{-1}. \tag{38}$$

References

Barnhart, C.J., Nimmo, F., Travis, B.J.: Martian Post-impact Hydrothermal Systems Incorporating Freezing. Icarus, Wroclaw (2010)

Bird, R.B., Stewart, W.E., Lightfoot, E.N.: Transport Phenomena, 2nd edn. Wiley, New York (1984)

Dempsey, D., Simmons, S.F., Archer, R., Rowland, J.: Delineation of catchment zones of geothermal systems in large-scale rifted settings. J. Geophys. Res. **117**, B10 (2012)

Deng, H., Stauffer, P.H., Dai, Z., Jiao, Z., Surdam, R.C.: Simulation of industrial-scale CO_2 storage: multi-scale heterogeneity and its impacts on storage capacity, injectivity and leakage. Int. J. Greenh. Gas Control **10**, 397–418 (2012)

Dodson, M.H.: Isenthalpic flow Joule–Kelvin coefficients and mantle convection. Nature **234**(5426), 212 (1971)

Fisher, A.T., Becker, K., Narasimhan, T.N., Langseth, M.G., Mottl, M.J.: Passive, off-axis convection through the southern flank of the Costa Rica Rift. J. Geophys. Res. **95**, 9343–9370 (1990)

Fisher, A.T., Hounslow, M.W.: Transient fluid flow through the toe of the Barbados accretionary complex: constraints from ocean drilling program leg 110 heat row studies and simple models. J. Geophys. Res. **95**, 8845–8858 (1990)

Haar, L., Gallagher, J., Kell, G.S.: NBS/NRC Steam Tables. Hemisphere, New York (1984)

Hanano, M.: A simple model of a two-layered high-temperature liquid-dominated geothermal reservoir as a part of a large-scale hydrothermal convection system. Transp. Porous Media **33**(1–2), 3–27 (1998)

Hayba, D.O., Ingebritsen, S.E.: The computer model HYDROTHERM, a three-dimensional finite-difference model to simulate ground-water flow and heat transport in the temperature range of 0 to 1,200 degrees C, pp. 94–4045. Water-Resources Investigations–U.S. Geological Survey, WRI (1994)

Ingebritsen, S.E., Rojstaczer, S.A.: Controls on geyser periodicity. Science **262**(5135), 889–892 (1993)

Jorand, R., Fehr, A., Koch, A., Clauser, C.: Study of the variation of thermal conductivity with water saturation using nuclear magnetic resonance. J. Geophys. Res. **116**, B08208 (2011)

Kestin, J.: A Course in Thermodynamics, Revised Printing, vol. i. Hemisphere, Washington, D.C. (1979)

Kieffer, S.W., Delaney, J.M.: Isentropic decompression of fluids from crustal and mantle pressures. J. Geophys. Res. **84**, 1611–1620 (1979)

Landau, L., Lifshitz, E.: Course of Theoretical Physics, vol 6: Fluid Mechanics. Butterworth Heinemann, Oxford (1987)

Lewis, K.C., Lowell, R.P.: Numerical modeling of two-phase flow in the $NaCl - H_2O$ system: introduction of a numerical method and benchmarking. J. Geophys. Res. **114**(B5) (2009)

Lu, X., Kieffer, S.W.: Thermodynamics and mass transport in multicomponent, multiphase H_2O systems of planetary interest. Annu. Rev. Earth Planet. Sci. **37**, 449–477 (2009)

Manga, M., Kirchner, J.W.: Stress partitioning in streams by large woody debris, Water Resour. Res. **40**(5) Art. No. W05110 (2004)

Palguta, J., Schubert, G., Travis, B.: Fluid flow and chemical alteration in carbonaceous chondrite parent bodies. Earth Planet. Sci. Lett. **296**, 235–243 (2010)

Person, M., Raffensperger, J.P., Ge, S., Garven, G.: Basin-scale hydrogeologic modeling. Rev. Geophys. **34**(1), 61–87 (1996)

Pippard, A.B.: Elements of Classical Thermodynamics: For Advanced Students of Physics. Cambridge University Press, Cambridge, UK (1957)

Pruess, K.: On CO_2 fluid flow and heat transfer behavior in the subsurface, following leakage from a geologic storage reservoir. Environ. Geol. **54**, 1677–1686 (2008)

Pruess, K., Wang, J.S.Y., Tsang, Y.W.: On thermohydrologic conditions near high-level nuclear wastes emplaced in partially saturated fractured tuff: 2. Effective continuum approximation. Water Resour. Res. **26**(6), 1235–1248 (1990)

Rees, D.A.S., Storesletten, L.: The effect of anisotropic permeability on free convective boundary layer flow in porous media. Transp. Porous Media **19**(1), 79–92 (1995)

Stauffer, P., Bekins, B.A.: Modeling consolidation and dewatering near the toe of the northern Barbados accretionary complex. J. Geophys. Res. **106**(B4), 6369–6384 (2001)

Straus, J.M., Schubert, G.: Thermal convection of water in a porous medium: effects of temperature- and pressure-dependent thermodynamic and transport properties. J. Geophys. Res. **82**(2), 325–333 (1977)

Steam properties database: version 2.2, NIST/ASME (2002)

Travis, B., Feldman, W.C., Maurice, S.: A mechanism for bringing ice and brines to the near surface of Mars. J. Geophys. Res. **118**, 2180–2197 (2013)

Travis, B.J., Janecky, D.R., Rosenberg, N.D.: Three-dimensional simulation of hydrothermal circulation at midocean ridges. Geophys. Res. Lett. **18**(8), 1441–1444 (1991)

Travis, B.J., Palguta, J., Schubert, G.: A whole-moon thermal history model of europa: Impact of hydrothermal circulation and salt transport. Icarus **218**, 1006–1019 (2012)

Travis, B.J., Rosenberg, N.D., Cuzzi, J.N.: On the role of widespread subsurface convection in bringing liquid water close to Mars' surface. J. Geophys. Res. **108**(E4) (2003)

Travis, B.J., Schubert, G.: Hydrothermal convection in carbonaceous chondrite parent bodies. Earth Planet. Sci. Lett. **240**(2), 234–250 (2005)

Tsang, C.: Linking thermal, hydrological, and mechanical processes in fractured rocks. Annu. Rev. Earth Planet. Sci. **27**, 359–384 (1999)

Voss, C.I.: A finite-element simulation model for saturated-unsaturated, fluid-density- dependent ground-water flow with energy transport or chemically-reactive single-species solute transport, pp. 84–4369. Water-Resources Investigations–U.S. Geological Survey, WRI (1984)

Waldbaum, D.R.: Temperature changes associated with adiabatic decompression in geological processes. Nature **232**(5312), 545–547 (1971)

Weir, G.J.: The relative importance of convective and conductive effects in two-phase geothermal fields. Transp. Porous Media **16**(3), 289–298 (1994)

Wood, S.A., Spera, F.J.: Adiabatic decompression of aqueous solutions: applications to hydrothermal fluid migration in the crust. Geology **12**, 707–710 (1984)

Zyvoloski, G.A.: Fehm: A control volume finite element code for simulating subsurface multi-phase multi-fluid heat and mass transfer, Los Alamos National Laboratory document LA-UR-3359, (2007)